THE JOURNAL OF PHYSICAL CHEMISTRY B

ARTICLE

pubs.acs.org/JPCB

Photoionization and Time-Dependent Stokes Shift of Coumarin 307 in Soft Matter: Solvation and Radical-Ion Pair Recombination Dynamics

Namasivayam Dhenadhayalan, Chellappan Selvaraju,* and Perumal Ramamurthy

National Centre for Ultrafast Processes, University of Madras, Chennai- 600 113, India

Supporting Information

ABSTRACT: Photoionization, fluorescence time-dependent Stokes shift (TDSS), and rotational dynamics of coumarin 307 (C307) have been investigated in soft matter system such as micelles using time-resolved transient absorption and fluorescence spectroscopy. Photoionization of C307 leads to the formation of coumarin radical cation and hydrated electron, which were characterized by their respective transient absorption. The photoionization yields are significantly higher in anionic sodium dodecyl sulfate (SDS) micelle than in cationic cetyltrimethylammonium bromide (CTAB) and neutral Triton X-100 (TX-100) micelles, indicating the influence of micellar surface charge on the efficient separation of radical cation-hydrated electron pair. The CTAB micelle favors the recombination of radical cation and hydrated electron leading to the formation of triplet state of C307, which causes a decrease in the photoionization yield. C307 exhibits TDSS in all micelles; the time evolution and the magnitude of the TDSS depend on nature of the micelle. In TX-100 micelles, the decay of the TDSS exhibits ultraslow component (165 ns) and is affected by the presence of electron scavengers. The ultraslow component in TX-100 micelle originates from the recombination of radical cation−hydrated electron, which results in the formation of twisted intramolecular charge transfer (TICT) state; such formation of TICT state was not observed in SDS and CTAB micelles. To the best of our knowledge, this is the first report where the radical-ion pair recombination dynamics is probed using TDSS in combination with time-resolved transient absorption studies. The activation energy for the solvent relaxation and radical-ion pair (solvent separated) recombination process was found to be 6.1 and 3.0 kcal mol^{-1}, respectively. Temperature effect on TDSS in TX-100 micelles confirmed the increase in the water hydration, and size of the micelle influences the relative contribution of the solvation and radical-ion pair recombination dynamics toward the total TDSS. We propose that TDSS observed in neutral micelles and reported in other biomolecules such as proteins by the 7-amino coumarin probe is not only due to the solvation dynamics alone but also due to the radical-ion pair recombination dynamics.

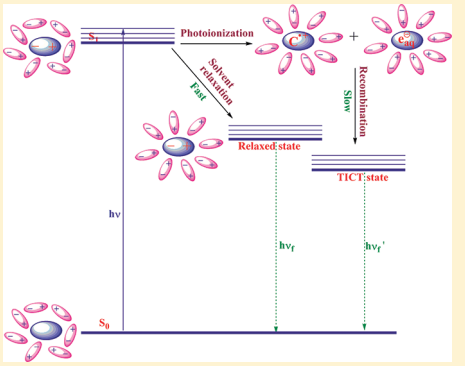

INTRODUCTION

Photoionization of solute molecules in water generates transient radical ion-electron pair that undergoes recombination or diffusional escape to the bulk water typically on the picosecond time scale. One of the most important issues surrounding the dynamics of the hydrated electron is electron−cation recombination process.[1] The photoelectron gets hydrated on the <1 ps time scale, and the hydrated electron plays an important role in many chemical and biological processes.[2−8] The photoionization processes in soft matter systems provide an inspiration to understand the complex biological processes. The soft matter systems are made up of molecular assemblies, which are self-organized; they have many different length scales from atomic (nanometers) to microscopic (millimeters), and their dynamics exhibits many different time scales from femtosecond to hours. The well-established soft matter systems include micelles, reverse micelles, vesicles, liquid crystals, cyclodextrin, polymers, and so on.[9,10] Micelles are considered as a simplest model for the biological system, and the studies on the photoionization and charge migration processes in the micellar system is applicable to the biological system and were also extended to solar energy harvesting systems.[11,12] The study of photoionization of chromophores in micelles continues to be a thriving research field in chemistry. Micellar systems are known to promote differential distribution of substrates, intermediates, and products in organic, aqueous, or interface regions, which can usually be explained by a combination of electrostatic and hydrophobic effect.[13−15]

The water molecules present in the biological system behave differently, which is responsible for the several unique functionality of the biological system.[16−18] Confinement of water molecules by the organized assemblies can lead to very slow solvation dynamics.[19−22] The solvation dynamics at the biological interface and organized assemblies have been studied by means of nuclear magnetic resonance (NMR),[23] magnetic relaxation dispersion (MRD),[24] neutron scattering,[25] photon echo,[26] and computer simulations.[27,28] Time-dependent Stokes shift (TDSS) measurement is a powerful spectroscopic technique to characterize dynamics of the solvent as well as complex condensed phases.[17,29,30] The TDSS monitors the interaction energy of a

Received: April 3, 2011
Revised: August 11, 2011
Published: August 12, 2011

Scheme 1. Structure of Coumarin 307

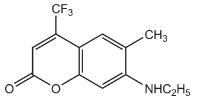

fluorescent probe with its molecular environment. The charge distribution of the probe is altered by electronic excitation, and the ensuing readjustment of the environment is reflected in the TDSS. In biological systems, the interaction energy of the fluorophore is influenced by the electrostatic potential increases due to the nearby water molecules, polar head groups, and counterions.

TDSS of a free probe in homogeneous solution exhibits a fast solvation component due to inertial motion and slow solvation component due to diffusive motion of the solvent; this corresponds to the longitudinal relaxation time of the solvent.[31] When the probe molecule attached to biomolecules such as protein or encapsulated in micelles, the TDSS exhibits one or more slow decay components in the addition to the diffusive component. The molecular origin of the longest decay component (10 ps to several nanoseconds) shown by the biomolecules and micelles is of utmost importance and enormous research has been carried out. Bhattacharyya[18] has concluded from the TDSS in micelles that the diffusive motion of the water molecules hydrating the surfactant aggregates is dramatically slow when compared with bulk water, typically by one to three orders of magnitude. Nandi et al.[32,33] concluded that the slow TDSS is due to the exchange of bound water to free water molecule. Zewail and coworkers reported that the long decay times characterize the water motions in the protein hydration layer, either exchange between hydration and bulk water or more subtle local rearrangements of the orientation and density of hydration water.[34−37] Nilsson et al.[28] studied the origin of the TDSS from a tryptophan residue in a protein using molecular dynamics simulations. They reported that after a few picoseconds the TDSS reflects the collective water displacement by the slowly fluctuating protein groups and does not reflect the individual motion of the water molecule. The origin of the slow TDSS at the biomolecular interfaces is explained so far due to modification of the hydrogen bonding network and structure of the water molecules in the vicinity of the biomolecules, transition of bound to free water molecules, and collective conformational dynamics of the biomolecules. There is no general consensus still regarding the origin of the slow evolution of TDSS displayed by the probe molecules encapsulated in micelles and in other biomolecules. In this Article, we propose a new molecular origin that arises because of the photoionization of the probe for the slow TDSS exhibited by the biomolecules and organized assemblies.

Photoionization, fluorescence TDSS, and anisotropy of C307 (Scheme 1) in SDS, CTAB, and TX-100 micelles are studied using time-resolved transient absorption and fluorescence spectroscopy. On excitation, C307 undergoes photoionization, which results in the formation of coumarin radical cation and hydrated electron pair. The influence of micellar charge on the separation and recombination of the radical cation and hydrated electron are presented. The time-resolved emission spectra (TRES) of C307 in all micelles were constructed in the absence and presence of electron scavengers. The highlight of the present investigation is the influence of electron scavenger on the decay of the TDSS in neutral micelle, which confirms that the TDSS is due to the existence of both solvation and radical-ion pair recombination dynamics. The effect of temperature on the TDSS in TX-100 micelle confirms the existence of Arrhenius type of activation energy barrier for both solvation and radical-ion pair recombination dynamics. The activation energy barrier for the radical-ion pair recombination is less than the activation energy barrier for solvation processes. From the present study, we emphasize that the radical-ion pair recombination may be one of the origins for the observed ultraslow dynamics and multiexponential decay of the TDSS exhibited by the probe present in the vicinity of the biomolecules and organized assemblies.

EXPERIMENTAL SECTION

Laser grade C307 was purchased from Exciton and used as received. Surfactants SDS and CTAB used for the preparation of micelles were of molecular biology grade purchased from SRL and Lancaster chemicals, respectively. TX-100 was purchased from Aldrich, and all surfactants were used without any purification. Chloranil and *trans*-stilbene were purchased from Merck. Triply distilled water was used to prepare micellar solutions. Coumarin dyes are reasonably soluble in the micellar solution. For all studies, the concentration of SDS, CTAB, and TX-100 were kept constant at ∼60 mM well above the CMC. The critical micellar concentration (CMC) of the surfactants SDS, CTAB, and TX-100 are 8.3, 0.80, and 0.24 mM, respectively.[13,38,39] The average aggregation number of SDS, CTAB, and TX-100 micelles is 62, 92, and 100, respectively.[13,38,39] The total coumarin concentration in the solution was kept at ∼10 μM.

The absorption spectra of the samples were recorded using an Agilent 8453 UV−visible diode array spectrophotometer. The fluorescence spectral measurements were carried out using Fluoromax-4 spectrophotometer (Horiba Jobin Yvon). Transient absorption experiments were carried out using nanosecond laser flash photolysis (applied photophysics). The third harmonic (355 nm) of a Q-switched Nd:YAG laser (Quanta-Ray, LAB 150, spectra physics) with 8 ns pulse width and 150 mJ pulse energy was used to excite the samples. The transients were probed using a 150 W pulsed Xenon lamp, a Czerny-Turner monochromator, and Hamamatsu R-928 photomultiplier tube as detector. The transient signals were captured with an Agilent infiniium digital storage oscilloscope, and the data were transferred to the computer for further analysis. For laser flash photolysis studies, samples were purged with either argon or N_2O gas for 45 min prior to the laser irradiation.

Time-resolved fluorescence decays were obtained by the time-correlated single-photon counting (TCSPC) technique with microchannel plate photomultiplier tube (Hamamatsu, R3809U) as detector and femtosecond laser as an excitation source. The second harmonics (400 nm) output from the mode-locked femtosecond laser (Tsunami, Spectra Physics) was used as the excitation source. The instrument response function for TCSPC system is ∼50 ps. The data analysis was carried out by the software provided by IBH (DAS-6), which is based on reconvolution technique using nonlinear least-squares methods. TRES spectra were generated from a set of emission decay times taken at 10 nm intervals spanning the fluorescence spectrum. The

Table 1. Absorption, Fluorescence Maximum, and Fluorescence Lifetime of C307 in Solvents and Micelles

solvents and micelles	λ_{abs} (nm)	λ_{emi} (nm)	τ (ns)	dielectric constant, ε
water	403	505	4.33	80.10
acetonitrile	387	478	5.17	36.64
methanol	393	493	5.20	33.0
ethanol	395	490	5.21	25.3
n-propanol	396	487	5.25	20.8
dichloromethane	384	456	4.74	8.93
chloroform	383	452	4.39	4.81
hexane	365	419	3.84	1.89
SDS	401	498	5.80	
CTAB	405	498	5.20	
TX-100	398	494	6.03	

TRES were constructed using steady-state emission intensity and fluorescence decay parameters following the procedure described by Maroncelli et al.[40] The solvation dynamics is described by the decay of the solvent correlation function, $C(t)$ defined as

$$C(t) = \frac{\nu_t - \nu_\infty}{\nu_0 - \nu_\infty} \quad (1)$$

where $\nu(0)$, $\nu(t)$, and $\nu(\infty)$ are the frequencies of fluorescence maximum at time zero, t, and infinity, respectively. The time zero is defined as the time when a probe is excited by a laser pulse, and the time infinity is defined as the time when the system achieves the equilibrium state. The $\nu(\infty)$ values had been taken to be the emission frequency beyond which an insignificant or no spectral shift was observed. The amount of missing component in the solvation dynamics is calculated by using the method proposed by Fee and Maroncelli.[41] The time zero frequency maximum can be estimated from the steady-state absorption and fluorescence spectra

$$\nu_{p,md}(t = 0) \approx \nu_{p,md}(abs) - [\nu_{np,md}(abs) - \nu_{np,md}(fl)] \quad (2)$$

where the subscripts "p" and "np" refer to the polar and nonpolar solvent, respectively, and here the frequencies are not the values at maxima but correspond to the midpoint frequencies (ν_{md}) in the solvent. The extent of the missing component is then determined by the value of $[(\nu_{cal}(0) - \nu(0))/(\nu_{cal}(0) - \nu(\infty))]$.

Time-resolved area normalized emission spectra (TRANES) were constructed by normalizing the area of each TRES spectrum such that the area of the spectrum at time t is equal to the area of the spectrum at the shortest t. Area normalized spectra were performed using the Peakfit v4.12 software.

Fluorescence anisotropy studies were carried out by measuring the polarized fluorescence decays, $I_{||}(t)$ and $I_{\perp}(t)$. From $I_{||}(t)$ and $I_{\perp}(t)$ decays, the anisotropy decay function $r(t)$ was constructed using the following relation

$$r(t) = \frac{I_{||}(t) - GI_{\perp}(t)}{I_{||}(t) + 2GI_{\perp}(t)} \quad (3)$$

where $I_{||}(t)$ and $I_{\perp}(t)$ are fluorescence intensity decays for parallel and perpendicular polarizations with respect to vertically polarized excitation light respectively. G is a correction factor for the polarization bias of the detection setup. The G factor was independently determined by using the horizontally polarized excitation light and measuring the two perpendicularly polarized fluorescence decays with respect to the excitation polarization.

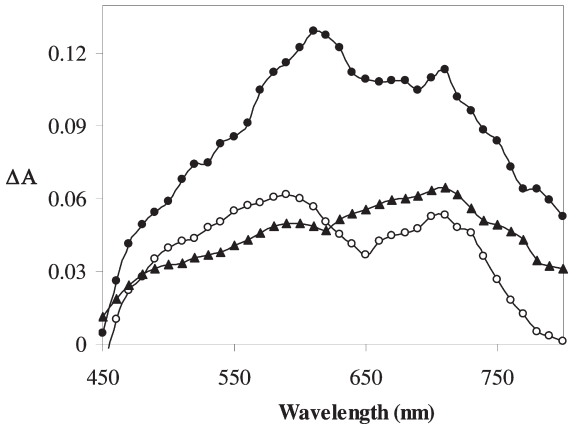

Figure 1. Transient absorption spectra of C307 in SDS (●), CTAB (○), and TX-100 (▲) micelles under argon saturation conditions recorded at 1 μs after the laser pulse (λ_{ex} = 355 nm).

RESULTS

Steady-State Absorption and Fluorescence Studies. Absorption and fluorescence spectra of C307 were recorded in SDS, CTAB, and TX-100 micelles and also in different solvents to understand the probable location of C307 in micelles. The absorption and fluorescence maximum of C307 was found to be dependent on the solvent polarity and the hydrogen bonding ability of the solvents. The absorption and fluorescence maxima of C307 in different solvents and micelles are given in Table 1. On excitation, C307 undergoes intramolecular charge transfer (ICT) from the electron-donating amino group to the electron-withdrawing carbonyl group. The absorption and fluorescence maxima were blue-shifted on decreasing the solvent polarity. In the case of alcoholic solvents, the absorption and fluorescence maxima were red-shifted compared with that of acetonitrile, even though acetonitrile is more polar than alcohols used in the present study. This is attributed to the hydrogen bonding interaction between the alcohols and amino or carbonyl group of the coumarin dye.[42,43] The absorption maximum of C307 in all micelles is more or less identical to that observed in water. The fluorescence maximum of C307 is blue-shifted in micelles compared with that of water, which indicates that the coumarin dyes are located in the less polar environment of the micellar medium compared with water.

Time-Resolved Transient Absorption Studies. Transient absorption spectra of C307 in micelles have been recorded on excitation at 355 nm under argon and N_2O saturated conditions is shown in Figures 1 and 2, respectively. In SDS and TX-100 micelles, C307 exhibits a broad absorption in the wavelength range 450−750 nm with the maxima at 610 and 710 nm. The transient absorption peak observed at 710 nm was found to disappear in the presence of N_2O (electron scavenger) and hence it is assigned to the absorption of the hydrated electrons.[44] The photoionization of C307 results in the formation of radical cation and hydrated electron. The transient absorption peak observed at 610 nm is due to the formation of coumarin radical cation.[44] To confirm the absorption of coumarin radical cation, laser flash photolysis of chloranil was carried out in the presence of low concentration of C307 in methanol. The photoinduced electron

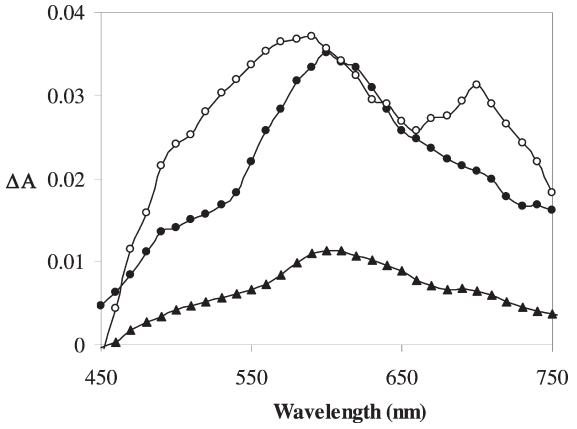

Figure 2. Transient absorption spectra of C307 in SDS (●), CTAB (○), and TX-100 (▲) micelles under N_2O saturation conditions recorded at 1 μs after the laser pulse (λ_{ex} = 355 nm).

transfer between the ground-state coumarin to the excited-state chloranil results in the formation of coumarin radical cation with weak transient absorption at 610 nm[45] (Supporting Information, Figure S1). The transient absorption observed in SDS and TX-100 micelles in the region of 550−750 nm is due to both radical cation and hydrated electron. The lifetime of hydrated electron in both the micelles is found to be 3.5 μs.

The transient absorption spectrum of C307 in CTAB micelles shows absorption maxima at 590 and 710 nm. The transients observed at 590 and 710 nm have short-lived and long-lived components. In the presence of N_2O, the transient absorbance decreases without change in the transient's maximum. The short-lived components observed at both the transient maxima were found to disappear in the presence of N_2O. This reveals that the short-lived component observed at 710 nm transients is attributed to the hydrated electron. The lifetime of the hydrated electron is found to be ~600 ns. The short-lived component at 590 may be due to both cation radical and hydrated electron. The observed short lifetime of the hydrated electron is probably due to facilitation of radical cation and hydrated electron recombination. The long-lived components at 590 and 710 nm were not affected by N_2O but are quenched in the presence of triplet quencher like *trans*-stilbene.[46] The broad transient absorption with maxima in the region of 590 and 710 nm is due to the triplet−triplet absorption of C307, and both of the decay rate constants are similar (1.89×10^4 s^{-1}). Jones II et al.[47] and Dempster et al.[48] have previously reported on the triplet−triplet absorption of coumarin in homogeneous solvents, and their findings are in line with our experimental results. In CTAB micelles, the coumarin radical cation absorption at 610 nm could not be observed clearly even in the presence of electron scavenger because of the overlap of the strong triplet−triplet absorption and the short lifetime of the radical cation due to the recombination. The separation and recombination of the radical-ion pair is greatly influenced by the charge of the micellar Stern layer, which in turn affect the photoionization efficiency of the C307 in micelles. The photoionization efficiency was estimated from the absorbance of the hydrated electron at 710 nm (measured at 200 ns after the laser pulse), the molar extinction coefficient of hydrated electron at this wavelength (ε_{710} = 18 000 M^{-1} cm^{-1}),[44] and the concentration

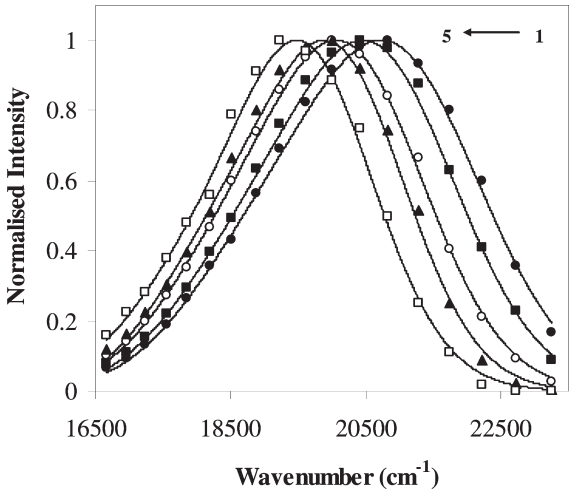

Figure 3. Time-resolved emission spectra of C307 in TX-100 at (1) 0 (●), (2) 0.5 (■), (3) 3 (○), (4) 20 (▲), and (5) 100 ns (□). The points in the spectra correspond to the experimental values and the solid lines correspond to the log-normal fits to the experimental data values.

of C307 (10 μM) using the following expression[49]

$$\mathrm{PI}(\%) = \frac{100\ \Delta A_{710}}{\varepsilon_{710}[\mathrm{C307}]} \quad (4)$$

The calculated photoionization efficiency of C307 is 94, 7, and 41% in SDS, CTAB, and TX-100 micelles, respectively. The effect of laser pulse energy on the formation of hydrated electron was studied in all micellar solution to examine whether the photoionization process is monophotonic or multiphotonic in nature. The plot of absorption of hydrated electron against pulse energy is found to be linear in all micellar solutions (Supporting Information, Figure S2). The slope values are close to unity, and thus the photoionization of C307 is monophotonic process in all micellar systems.

Time-Resolved Fluorescence Studies. The fluorescence decay of C307 in all the micelles exhibits a single exponential decay at their emission maximum. This indicates that the different C307 molecules present in different micelles in particular micellar solution experience similar microenvironments. The fluorescence lifetimes of C307 in SDS, CTAB, and TX-100 micellar solution were found to be 5.83, 5.20, and 5.91 ns, respectively. There is no observable change in the fluorescence lifetime in the presence of electron scavengers (N_2O, H^+) in all micellar solutions. C307 exhibits wavelength-dependent fluorescence decay in all micelles, which indicates the TDSS in the emission spectra. The fluorescence decay observed at the red edge of the emission spectrum exhibits a distinct growth in all micelles, which indicates that the C307 undergoes either solvation or excited state reaction. Typical TRES for C307 in TX-100 micelles at room temperature is shown in Figure 3.

The decay of $C(t)$ of C307 in SDS, CTAB, and TX-100 micelles are presented in Figures 4 and 5. The decay of $C(t)$ and dynamic spectral shift ($\Delta\nu$) is found to be dependent on the nature of the micelles. In SDS micelles, the decay of $C(t)$ follows single exponential function, whereas the $C(t)$ decay follows multiexponential function in CTAB and TX-100. The decay characteristics of $C(t)$ of C307 in all micelles are summarized in Table 2. In SDS and CTAB micelles, the observed $\Delta\nu$ is very small compared with TX-100 micellar solution. The very low value of $\Delta\nu$ in SDS and

CTAB micelles reflects that the large portion of the ultrafast component in the TDSS is missed because of the finite time resolution of the TCSPC setup (~50 ps). The estimation of real-time zero fluorescence maximum of C307 in micelles may give the information on the missing component in the solvation dynamics. The missing component in SDS, CTAB, and TX-100 micelles are found to be 89, 80, and 28%, respectively. In SDS and CTAB micelles, most of the solvation processes are completed on a subpicosecond time scale and could not be observed with the present instrumental setup. Hence, a substantial amount of the fast decay component of solvation dynamics remains undetected in our time-resolved measurements.

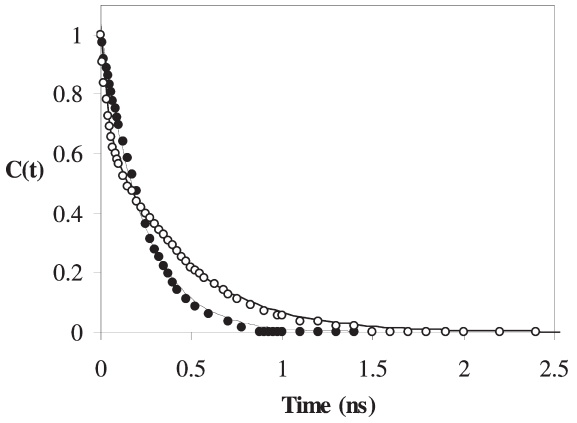

Figure 4. Decay of $C(t)$ of C307 in SDS (●) and CTAB (○) micelles. The points denote the experimental values of $C(t)$ and the solid lines denote the best fit to a exponential decay.

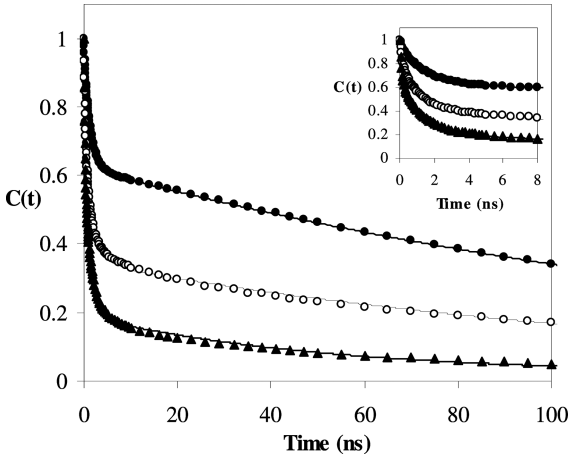

Figure 5. $C(t)$ decay of C307 in TX-100 micelle in air equilibrated (●), N_2O saturated (○), and acidic condition pH 2.0 (▲). The inset shows the same for initial parts of the decays of $C(t)$.

The photoionization of C307 is clearly established in the time-resolved transient absorption studies. Photoionization of C307 results in the formation of radical cation and hydrated electron, and the micellar charge plays an important role in the separation of the photoionization products. The decay of $C(t)$ in TX-100 micelle displays an unusual ultraslow decay component in the TDSS. To understand the effect of recombination of the photoionization products on the TDSS in micelles, we have carried out the time-resolved fluorescence measurements in the presence of electron scavengers (N_2O and H^+). The $C(t)$ decay of C307 in TX-100 micelles under N_2O saturated and at pH 2.0 is shown in the Figure 5. The decay characteristics of $C(t)$ in the presence of electron scavenger for all micelles are summarized in Table 3. The presence of electron scavenger does not influence the $C(t)$ decay in SDS and CTAB micelles, whereas the ultraslow component relaxation time and amplitude decreases in TX-100 micelles.

The temperature effect on $C(t)$ decay was carried out for the TX-100 micelles. In SDS and CTAB micelles, the observed Stokes shift is much less (<200 cm^{-1}), so it is not possible to study the effect of temperature on $C(t)$ decay in these micelles. The decays of $C(t)$ in TX-100 micelles in the temperature range of 283−328 K are shown in Figure 6. Throughout the temperature range, the $C(t)$ decay is well-fitted by triexponential function (Table 4). For all three components, the decay time decreases with increasing temperature. The amplitude of τ_1 and τ_2 increases, whereas that of τ_3 decreases with increasing temperature except in the temperature range of 295 K.

Time-Resolved Anisotropy Studies. To get more insight into microenvironments around the probe and thus to have a better understanding of the nature of the $C(t)$ decay, fluorescence anisotropy of C307 was measured in all micelles. The representative anisotropy decays of C307 in all micelles are shown in Figure 7, and the decay parameters are listed in Table 5. The anisotropy decays were fitted with a biexponential function with fast (τ_{r1}) and slow (τ_{r2}) rotational relaxation time in all micelles. Similar biexponential behavior reported in the literature for these micellar systems using different coumarin probes.[50,51] The rotational relaxa-

Table 2. Decay Characteristics of $C(t)$ of C307 in Micelles

micelles	ν_0 (cm^{-1})	ν_∞ (cm^{-1})	$\Delta\nu$ (cm^{-1})	τ_1 (ns)[a]	a_1 (%)	τ_2 (ns)[a]	a_2 (%)	τ_3 (ns)[a]	a_3 (%)	$\langle\tau\rangle$ (ns)[b]
SDS	20098.09	19965.13	132.96					0.230	100	0.230
CTAB	20090.70	19887.57	203.13			0.029	29	0.422	71	0.308
TX-100	20721.02	18835.58	1885.44	0.14	04	1.37	34	165.06	62	102.80

[a] Error in the results ±10%. [b] $\langle\tau\rangle = \Sigma a_i\tau_i$

Table 3. Decay Characteristics of $C(t)$ of C307 in the Presence of Electron Scavenger in Micelles

micelles	ν_0 (cm^{-1})	ν_∞ (cm^{-1})	$\Delta\nu$ (cm^{-1})	τ_1 (ns)[a]	a_1 (%)	τ_2 (ns)[a]	a_2 (%)	τ_3 (ns)[a]	a_3 (%)	$\langle\tau\rangle$ (ns)[b]
SDS-N_2O	20048.59	19936.52	112.07					0.228	100	0.228
CTAB-N_2O	20114.51	19962.89	152.62			0.035	33	0.496	67	0.343
TX100-N_2O	20767.17	19521.19	1245.97	0.12	18	1.27	47	127.54	35	45.26
TX100-pH 2.0	20875.94	19751.93	1124.01	0.13	37	1.46	46	50.52	17	9.31

[a] Error in the results ±10%. [b] $\langle\tau\rangle = \Sigma a_i\tau_i$.

tion times in all micelles are higher than that of pure water (108 ps), which indicates that the rotational relaxation process is much slower in micelles compared with water. This fact strongly suggests that the C307 molecules are located in a confined environment, where the motion is drastically hindered. Three different kinds of motions can contribute to the anisotropy decay in micellar solutions.[52−54] These are (i) the wobbling motion of the probe in the micellar interface layer, (ii) the lateral diffusion of the probe along the micellar surface, and (iii) the rotational motion of the whole micelle. The biexponential behavior of the probe in micelles can be explained using a two-step model and wobbling-in-a-cone model. As treated in a two-step model, the experimentally measured τ_{r1} and τ_{r2} values are determined by the correlation times for the wobbling motion (τ_W), lateral diffusion (τ_L), and the whole micelle rotation (τ_m) as follows

$$\tau_{r1}^{-1} = \tau_W^{-1} + \tau_{r2}^{-1} \quad (5)$$

$$\tau_{r2}^{-1} = \tau_L^{-1} + \tau_m^{-1} \quad (6)$$

For all micelles, the τ_m values can approximately be estimated using the Stokes−Einstein−Debye equation as[52−54]

$$\tau_m = \frac{4\pi r_m^3 \eta}{3k_B T} \quad (7)$$

where η is the viscosity of water (0.89 cP), k_B is the Boltzmann's constant, and r_m is the radius of the micelle. The τ_m values are estimated to be in the range of a few tens of nanoseconds and much higher than the rotational times (τ_{r1} and τ_{r2}) obtained from the anisotropy decays. This indicated that the contribution of the whole micelle rotation to the observed anisotropy decay is negligible. We have also calculated the order parameter (S) to get a clear idea about the location of the probe. The value of S is obtained from the relative amplitude of the slow component (a_{r2}) as

$$S = \sqrt{a_{r2}} \quad (8)$$

The magnitude of the S is a measure of spatial restriction and has values from 0 (unrestricted motion) to 1 (completely restricted motion). If the probe resides in the micellar core, the expected S value is close to zero and the anisotropy decay is single-exponential.[52−54] In the present systems, the estimated S values are close to 1 in all micelles (Table 5). The higher value of the order parameter indicates the restricted motion of C307 in all micelles and preferentially resides in the Stern/palisade layer of the micelle. It is seen that the τ_{r2} values are 8−10 times higher than the τ_{r1} values. Therefore, the τ_{r1} and τ_{r2} components are determined by the wobbling motion and later diffusional motion of the probe in the micellar interface layer, respectively. In all micellar systems, the low value of initial anisotropy (r_0) suggests that the fast component of anisotropy decay is not resolved in our picosecond set up. The missed fast initial portion of anisotropy decay may be due to fast wobbling motion of the C307 in all micelles.

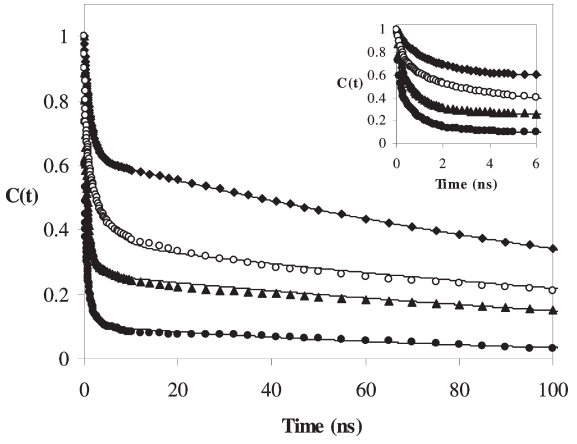

Figure 6. Effect of temperature on the $C(t)$ decay of C307 in TX-100 micelles: 283(○), 298 (◆), 313 (▲), and 328 K (●). The inset shows the same for initial parts of the decays of $C(t)$.

DISCUSSION

In micelles, there are three possible location of C307, namely, bulk aqueous phase, Stern/palisade layer, and hydrocarbon core layer. Both steady-state absorption and fluorescence studies indicate that the C307 in micelles experiences a polarity different from the bulk water and hydrocarbon core region of the micelles. The fluorescence maximum of C307 is blue-shifted in micelles compared with water, and the fluorescence maximum is nearly identical to that of alcoholic solvents. The micropolarity of the micellar interface layer is very close to the polarity of the methanol.[55] This confirms that the C307 molecules are residing in the Stern/palisade layer of the micelles.[39,55,56] The slow rotational relaxation of C307 in all micelles and higher value of order parameter (S) in the fluorescence anisotropy measurement confirms the location of the C307 in the Stern/palisade layer of the micelles.

Direct 355 nm laser excitation of C307 in all micelles gives rise to a transient absorption spectrum with contributions from (i) coumarin radical cation (610 nm), (ii) hydrated electron (710 nm), and (iii) triplet−triplet absorption of C307 (broad absorption with maxima at 590 and 710 nm). The lifetime and yield of the transient species strongly depend on the nature of the micelles. The picosecond pump−probe studies conclude that the photoionization and formation of hydrated electron take place within 50 ps in all micelles (Supporting Information, Figure S3). Migus et al.[57] studied the solvation dynamics of electron in water by photoionizing the solvents and reported that the formation of hydrated electron from the dry electron through the wet electron completes in ∼350 fs. This suggests that the hydration of the electron occurs in the Stern/palisade layer of the micelles. The initial photoionization of C307 associated with SDS micelle will generate hydrated electron, which is rapidly repelled from the

Table 4. Decay Characteristics of $C(t)$ of C307 in TX-100 Micelle at Different Temperatures

temp (K)	ν_0 (cm^{-1})	ν_∞ (cm^{-1})	$\Delta\nu$ (cm^{-1})	τ_1 (ns)[a]	a_1 (%)	τ_2 (ns)[a]	a_2 (%)	τ_3 (ns)[a]	a_3 (%)	$\langle\tau\rangle$ (ns)[b]
283	20902.31	19468.46	1433.86	0.34	32	3.47	32	202.60	36	74.15
295	20721.02	18835.58	1885.44	0.14	04	1.37	34	165.06	62	102.80
313	20730.91	19877.19	853.72	0.11	31	0.98	42	137.95	27	37.70
328	21020.98	20038.7	982.27	0.07	46	0.87	43	93.05	11	10.64

[a] Error in the results ±10%. [b] $\langle\tau\rangle = \Sigma a_i\tau_i$

dx.doi.org/10.1021/jp203092c |J. Phys. Chem. B 2011, 115, 10892–10902

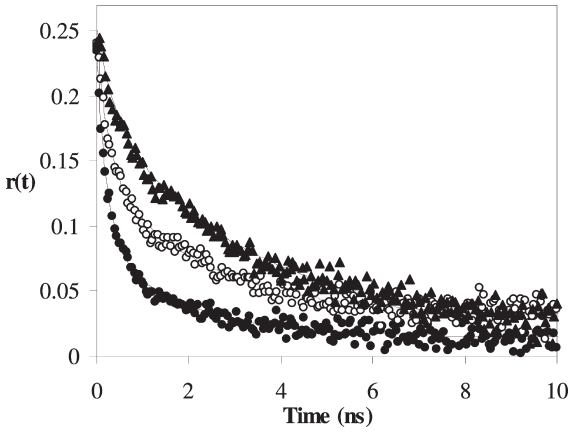

Figure 7. Fluorescence anisotropy decay of C307 in SDS (●), CTAB (○), and TX-100 (▲) micelles.

Table 5. Rotational Relaxation Times and Order Parameter Obtained from the Anisotropy Decays of C307 in Micelles

medium	r_0	τ_{r1} (ns)[a]	a_{r1} (%)	τ_{r2} (ns)[a]	a_{r2} (%)	$\langle\tau_r\rangle$ (ns)[b]	S
water	0.22	0.108	100			0.108	
SDS	0.23	0.223	19.71	1.79	80.29	1.48	0.89
CTAB	0.24	0.266	11.18	2.27	88.82	2.05	0.94
TX-100	0.24	0.309	3.46	3.03	96.54	2.94	0.98

[a] Error in the results ±5% [b] $\langle\tau_r\rangle = a_{1r}\tau_{1r} + a_{2r}\tau_{2r}$

negatively charged micellar Stern layer to the aqueous phase, whereas the coumarin radical cation is associated with the Stern layer due to the hydrophobic and electrostatic attraction, and this separation of the photoionization products leads to an enhanced photoionization yield in SDS micelles. In CTAB micelles, the hydrated electron gets attracted by the positive headgroup, whereas the radical cation also resides in the Stern layer due to the hydrophobicity, and hence the photoionization products were unable to separate and cause the recombination process. The recombination of radical cation and hydrated electron favors the formation of triplet state of C307 in CTAB micelle; hence, the yield of photoionization product is very low. The triplet state formation may be due to the presence of heavy atom (bromide counterions) in Stern layer of the CTAB micelles. To confirm the effect of heavy atom on the triplet induction, the transient absorption spectrum of C307 was recorded in methanol in the presence of heavy atom iodide. The resulting transient absorption spectrum shows 590 and 710 nm maximum similar to those observed in the CTAB micelles (Supporting Information, Figure S4). So, in CTAB micelle, the recombination of radical cation-hydrated electron and triplet induction by the bromide heavy atom results in the formation of a triplet state.

In TX-100 micelle, the radical cation and hydrated electron are diffused to large extent to each other because of large thickness of palisade layer. The TX-100 micelles do not have electrostatic effects at the palisade layer; the photoionization efficiency is lower in TX-100 micelle compared with SDS micelles. The photoionization of C307 is a monophotonic process in all micellar medium, which is confirmed by the effect of laser pulse energy on the hydrated electron absorption. The photoionization and subsequent photophysical process of C307 in micelles is schematically shown in Scheme 2.

Scheme 2. Photoionization and Subsequent Photophysical Processes of C307 in Micelles

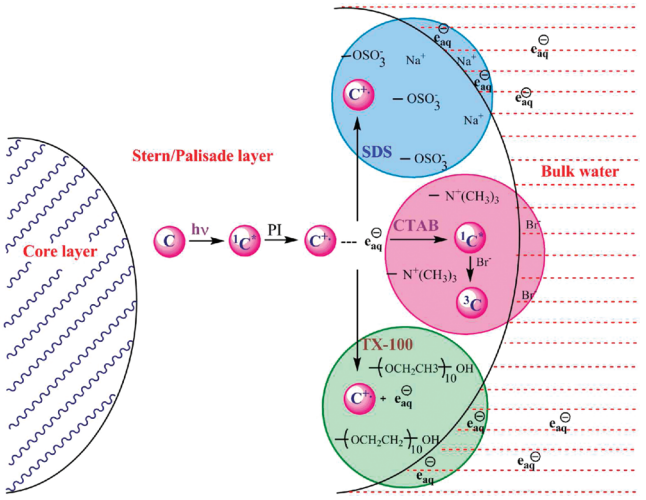

The TDSS of C307 in all micelles may be attributed to the solvation and excited-state dynamics of C307 in the Stern/palisade layer. The water molecules, counterions, alkyl chains, and the polar head groups of the surfactant are responsible for the solvation of instantaneously created C307 dipole in Stern/palisade layer of the micelles. As revealed from the electron spin resonance studies,[58] the dynamics of the alkyl chains in the micelles occur on very slow time scales on the order of 100 ns. Because the polar head groups are attached to long alkyl chains, the mobility of the polar head groups is restricted to a large extent. For the ionic micelles (SDS and CTAB), the counterions are quite immobile because of the stationary ionic head groups. The observed picosecond−nanosecond decay of the TDSS is not due to the counterions, alkyl chain, and polar headgroup of the surfactant molecules. The water molecules present in the wet Stern/palisade layer are the main influence for the solvation of C307 in all the micelles.

The $C(t)$ decay of C307 in TX-100 micelle exhibits triexponential decay with fast component (τ_1) of ∼140 ps, slow component (τ_2) of ∼1.37 ns, and an ultraslow component of ∼165.06 ns with an average lifetime of 102.8 ns. To the best of our knowledge, this is the first report for the triexponential behavior of $C(t)$ with an unusual slow component in TX-100 micelle. Solvation dynamics of TX-100 micelles using coumarin 480, coumarin 153, and coumarin 151 were extensively studied by Sarkar et al.[59] and Kumbhakar et al.[60] They reported the biexponential behavior of $C(t)$ with picosecond (200−700 ps) and nanosecond (2−4 ns) components. The unusual ultraslow component (τ_3 = 165 ns) displayed by C307 in TX-100 micelle is different from those reported using probes like coumarin 102, coumarin 151, and coumarin 153. From the transient absorption studies, we confirmed that on excitation C307 in micelles undergoes photoionization that results in the formation of radical cation and hydrated electron. The recombination of radical cation and hydrated electron is possible to occur in TX-100. In CTAB micelles, the recombination results in the triplet state, which is confirmed by strong triplet−triplet absorption, but the triplet−triplet absorption of C307 is very weak in TX-100 micelle compared with CTAB and indicates that the recombination results in a different state instead of triplet state. The solvation dynamics studies of

C307 in TX-100 micelle were carried out in the presence of electron scavengers (N_2O and H^+ ion) to confirm the effect of recombination on the observed dynamics in the TDSS. In the presence of electron scavenger, the decay times τ_1 and τ_2 do not change much, whereas the ultraslow component decay time (τ_3) and amplitude were drastically decreased. If this ultraslow component is due to the segmental chain dynamics, then it should not be affected in the presence of electron scavengers, but the ultraslow component decay time and relative amplitude were affected, which confirms that it is not due to the segmental chain dynamics of polyoxyethylene chain. The reaction of electron scavenger with hydrated electrons is given in eqs 9 and 10, which competes with recombination process, thereby decreasing the lifetime and amplitude of the ultraslow component. The rate constant for the recombination is found to be on the order of 10^6, whereas the rate constant for the electron-scavenging reactions[61] were reported to be on the order of 10^9.

$$e^{\Theta}_{aq} + N_2O \rightarrow OH^{\cdot} + OH^{-} + N_2 \quad (9)$$

$$e^{\Theta}_{aq} + H^{+} \rightarrow H \quad (10)$$

The kinetics of the TDSS in TX-100 micelles is very slow, and the relaxation processes are not complete within the experimental time window, which is given by the fluorescence lifetime (6 ns) of C307. To understand the kinetics of the relaxation processes, we used the value of the ν_∞, which is a limit for the time infinity of the exponential fit to the time dependence of ν_t. For TX-100 micelles, there is not much change in the observed ν_0 value in the presence of electron scavenger, whereas the ν_∞ value decreases ($\sim$900 cm^{-1}) in the presence of electron scavenger. The observed fluorescence maximum of the relaxed state of the C307 in SDS, CTAB, and TX-100 (in the presence of strong electron scavenger, H^+) is found to be very close to each other (503 $\pm$ 2 nm), but for TX-100 micelles, the relaxed state fluorescence maximum is found to be 531 nm in the absence of electron scavenger, which is $\sim$28 nm red-shifted compared with SDS, CTAB, and TX-100 (in the presence of strong electron scavenger). The observed additional Stokes shift ($\sim$900 cm^{-1}) in TX-100 micelles is due to the formation of new emissive state through the recombination of hydrated electron and radical cation.

Ghosh has reported that the recombination of radical cation and electron results in the relaxed state of coumarin 343 and observed the red-shifted emission from the relaxed state.[62] 7-Amino coumarins in highly polar solvents result in the twisted ICT state by twisting the amino group around C−N bond in the excited state.[63,64] Ramakrishna et al.[65] reported that the emission from the TICT state has been observed from the coumarin probe [D-1421] on the TiO_2 nanoparticles surface. The lifetime of the relaxed S_1 state of C307 in TX-100 micelles is found to be 5.91 ns, and also considering the slow relaxation of water molecules, the formation of the relaxed state is completed before 20 ns. This suggests that the new emissive state observed above 20 ns is not due to the relaxed state. The emissive state formed by the recombination of radical cation and hydrated electron is assigned to the TICT state. The photoionization results in the removal of one electron in the lone pair present in the amino group, which may facilitate the twisting of the C−N bond, leading to a nonplanar twisted conformation and recombination of radical cation and hydrated electron results in the TICT state. To confirm the formation of new TICT emissive state, we performed

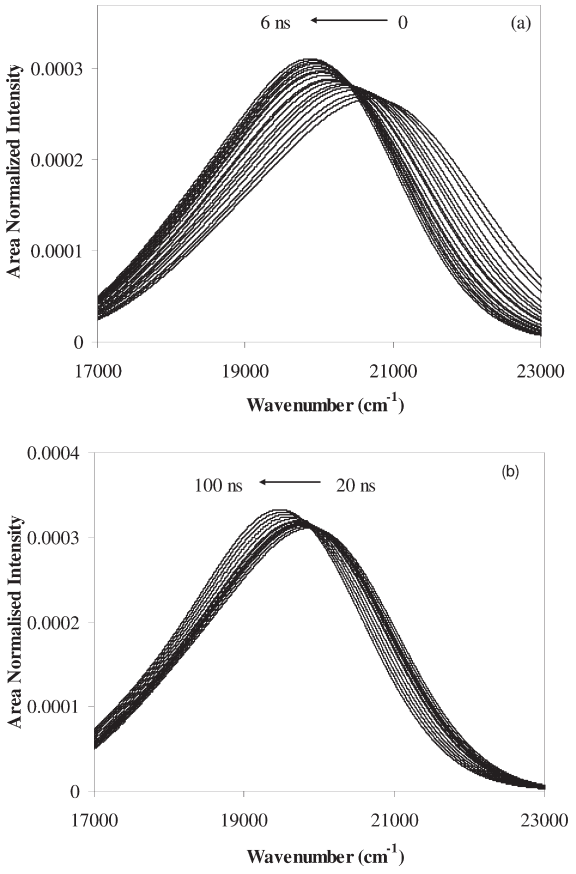

Figure 8. Time-resolved area normalized emission spectra of C307 in TX-100 micelles at time between (a) 0 to 20 ns and (b) 20 to 100 ns.

TRANES analysis for C307 in TX-100 micelles. From the TRANES analysis, we observed that up to 20 ns the emission maximum shifts continuously without any isoemissive point, which confirms the solvent relaxation of the ICT state. After 20 ns, an isoemissive point is observed in the TRANES spectrum, which confirms the presence of another emitting state apart from the relaxed state (Figure 8). Furthermore, to confirm the presence of TICT state in TX-100, we constructed the transient absorption spectra at 100 ns after the laser pulse and is shown in Figure 9. The transient spectrum shows a new transient absorption with a maximum at 480 nm along with the absorption of coumarin radical cation and hydrated electron in TX-100 micelles, which is not affected by the presence of oxygen. In the case of SDS and CTAB, there is no such new transient absorption observed at 480 nm. This 480 nm transient may be assigned to the absorption of TICT state. On longer time scale (>100 ns), TICT state absorption is mixed with strong absorption of hydrated electron and radical cation. On the basis of the above observation, we emphasize that the recombination of radical-ion pair leads to the formation of TICT state rather than in relaxed state in TX-100 micelles.

The ν_∞ value of C307 in TX-100 micelles increases (shifted to higher energy) in the presence of electron scavengers. It is due to the reaction of hydrated electron with the scavengers that prevents the slow formation of TICT state with lower energy. In the presence of electron scavenger, the relaxation process is completed at an earlier time when compared with that in the absence of electron scavenger. The increase in the ν_∞ value, the

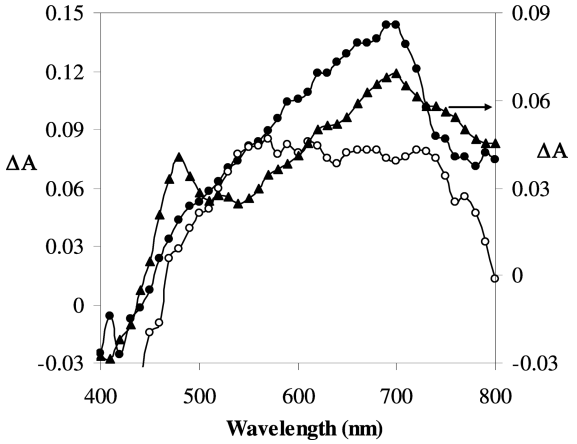

Figure 9. Transient absorption spectra of C307 in SDS (●), CTAB (○), and TX-100 (▲) micelles recorded at 100 ns after the laser pulse.

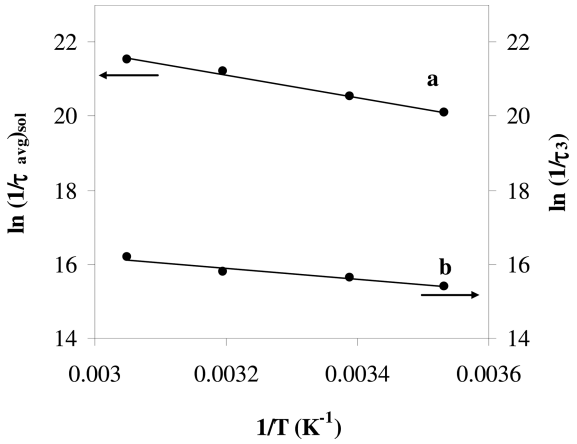

Figure 10. Plot of $1/T$ versus (a) $\ln(1/\tau_{avg})_{sol}$ and (b) $\ln(1/\tau_3)$.

time at which the ν_∞ extracted from the TRES affects the relaxation time and corresponding relative amplitude, and the concentration of the TICT state have no effect on the relaxation time and relative amplitude. The triexponential behavior of the solvent response function in TX-100 micelle is explained as follows. The two solvation components (140 ps and 1.37 ns) are due to the relaxation of the water molecules present in the palisade layer. The similar solvent relaxation times for TX-100 micelles were reported using C480 and C153, which gives further support for the above conclusion.[59,60] The ultraslow component (165 ns) is due to radical-ion pair recombination dynamics, which results in the formation of TICT state. The experimentally constructed decay of $C(t)$ from the TDSS of C307 in TX-100 micelle consists of both relaxation dynamics of water in the palisade layer and radical-ion pair recombination dynamics.

The $C(t)$ decay of C307 in TX-100 micelles at different temperature clearly shows a temperature effect on the solvation dynamics (τ_1 and τ_2) and radical-ion pair recombination dynamics (τ_3). The three decay times were found to decrease with increasing temperatures. The activation energy for the solvent relaxation process and the radical-ion pair recombination is calculated from the plot of $\ln(1/\tau_{avg})_{sol}$ versus $1/T$ and $\ln(1/\tau_3)$ versus $1/T$, respectively (Figure 10). The resulting plots were found to be linear, which indicates the Arrhenius dependence of the rate constant for the solvation and recombination processes. The activation energy for the solvation and recombination processes is found to be 6.1 and 3.0 kcal mol^{-1}, respectively. The recombination of radical cation and hydrated electron requires less activation energy than the solvent relaxation process, which confirms that the formation of TICT is possible through recombination. The estimated activation energy for the solvation processes reported here is very close to the value reported by Pal et al.[66] in the molecular simulation dynamics and by Sen et al.[67] using the TDSS of 4-AP in TX-100 micelle. According to computer simulation,[66] the hydrogen bond energy of water−micellar polar headgroup and water−water is reported to be ∼13 to 14 and ∼6 kcal mol^{-1}, respectively. The energy difference of a water−micellar polar headgroup and water−water hydrogen bond, that is, the energy difference between bound water and free water, is ∼7 to 8 kcal mol^{-1}. In the present study, the activation energy (6.1 kcal mol^{-1}) for the solvation process is in remarkably good agreement with hydrogen bond energy difference obtained from the simulation studies. Hence, this activation energy for the solvation dynamics is ascribed to the transition of bound water to free water molecules in micellar interface region and supports the bimodal relaxation of water molecules proposed by Nandi et al.[32]

It is evident from Table 4 that the contribution of the fast solvation component (τ_1) increases with the increase in temperature with an inversion at 295 K. Quasi-elastic light scattering studies[68] in TX-100 micelle reveal that the hydration number and micellar size increases from 6 to 16 and 30 to 83 Å, respectively, with increasing temperature from 283 to 323 K. The number of free water molecules in palisade layer increases with the increase in temperature, and the photoionization products are stabilized by the effective solvation. At 283 K, the number of water molecules in the palisade layer is not enough to solvate and stabilizes the photoionization products, which results in more geminate recombination. This is further supported by the decrease in the photoionization yield measured at 283 K using the hydrated electron absorbance at 710 nm. The photoionization yield in TX-100 micelle at 295 K was found to be 41%, whereas at 283 K the photoionization product yield decreases to 30%. As a consequence, the contribution of recombination toward the total TDSS decreases at low temperature, which results in inversion in the amplitude and average solvation time. The similar inversion in the average solvation time with temperature was reported by Kumbhakar et al.[60] by using C153 and C151 in TX-100 micelle, and they reported that the inversion may be due to the combined effect of the change in size and hydration of the micelle. The present study reveals that the increase in the hydration and size of the micelle does not have much influence on the activation energy barrier for the solvation and the recombination processes but influences their relative contribution toward the total time-dependent Stokes shift. At 328 K, the amplitude of the radical-ion pair recombination processes (a_3) decreases to 11% from 62% at 295 K, which may be due to escape of the hydrated electron from the palisade layer to the bulk aqueous phase and prevents the recombination at high temperature.

The $C(t)$ decay of C307 in CTAB micelles follows biexponential function, and the average solvation time is 308 ps. The similar solvent relaxation time was reported in CTAB using C480, 4-AP, and DCM.[59,69,70] The $C(t)$ decay of C307 in SDS micelles follows single exponential function with solvation time 230 ps. Vajda et al.[71] reported that the solvation time of C480 in water is 310 fs. The observed solvation time in all micelles is much slower compared with that of bulk water. The observed solvation time in SDS and CTAB micelles is much less than that

of TX-100 micelles; it is expected that there is more water penetration in the Stern layer of former micelles than that of later micelles. The observed TDSS in SDS and CTAB micelles is due to the dynamics of water molecules present in the Stern layer of the micelle. The unusual ultraslow component is not observed in both SDS and CTAB micelles. In SDS micelles, the recombination of coumarin radical cation and hydrated electron is prevented effectively because of the negative charge of the Stern layer. In the case of CTAB micelles, the radical-ion pair recombination leads to triplet state due to heavy atom induction. The decay of $C(t)$ is single exponential in SDS, whereas multiexponential behavior is observed in CTAB and TX-100 micelles. There is no recombination of the radical-ion pair in SDS micelle, and radical-ion pair recombination in CTAB and TX-100 micelles results in the excited singlet state. From the above discussion, we propose that the recombination of the radical-ion pair may be one of the reasons for the multiexponential decay of $C(t)$, and observed TDSS is not only due to the solvation dynamics alone but also due to the radical-ion pair recombination dynamics in neutral micelles and reported in biomolecules[72] by using the 7-amino coumarin probes.

Time-resolved anisotropy studies show that the rotational relaxation of C307 in micelles occurs at a much slower rate compared with pure water. The rotational relaxation time of τ_{r1} and τ_{r2} is attributed to the wobbling motion and lateral diffusion of the probe in the micellar interface region. In TX-100 micelles, rotational relaxation for the wobbling-in-cone and lateral diffusion are slower than that in SDS and CTAB, which may be due to the larger thickness of the palisade layer in TX-100 micelles. Comparing the solvation time with the rotational relaxation time, it is seen that the observed time constants of anisotropy are longer than the time constants of solvation process. In the study of solvation dynamics of supramolecular assemblies using C480 probe, Mandal et al.[73] reported the slow anisotropy decay compared with solvent relaxation. The anisotropy decay is determined by the wobbling and translational motion of the probe molecule along with overall rotation of the micelle, whereas the solvent relaxation is determined by the change in the orientation of the solvent molecules. This indicates that the origins of the solvation and anisotropy process are different from each other.

CONCLUSIONS

The present investigation confirms that the excited-state photoionization of C307 in all micelles leads to the formation of coumarin radical cation and hydrated electron as primary photoionization products. The separation and recombination of the photoionization products are influenced by the micellar charge, size, and counterions in the micellar Stern/palisade layer. In SDS micelle, there is no recombination of the photoionization products, whereas in CTAB and TX-100 micelles, the recombination of photoionization products results in the formation of triplet and TICT state, respectively.

C307 exhibits TDSS in all micelles; the time evolution and the magnitude of the TDSS depend on the nature of the micelles. In TX-100 micelles, the ultraslow component (165 ns) was due to the formation of TICT state through the recombination of the coumarin radical cation and hydrated electron, which is confirmed by the effect of electron scavenger on the decay of TDSS. In neutral micelles and biomolecular systems, the dynamics of radical-ion pair recombination also contributed to TDSS in addition to the solvation dynamics. The solvation and radical-ion pair recombination processes were found to be the activation energy barrier crossing type. The activation energy for solvation and radical-ion pair recombination processes was found to be 6.1 and 3.0 kcal mol^{-1}, respectively. The temperature effect on solvation dynamics reveals that the increase in the hydration and the size of the micelle does not have much influence on the activation energy barrier for the solvation and the recombination processes but influences their relative contribution toward the total TDSS. The recombination of radical-ion pair may be one of the origins for slow and multiexponential decay of the biological water relaxation. The recombination process does not influence the rotational relaxation of C307, and observed rotational relaxation is attributed to the wobbling and lateral diffusion of the coumarin in Stern/palisade layer.

ASSOCIATED CONTENT

Supporting Information. Nanosecond transient absorption spectrum of chloranil in the presence of C307 in methanol; the effect of laser pulse energy on the absorbance of hydrated electron in all micelles; picosecond pump−probe transient absorption spectra of C307 in micelles; transient absorption spectrum of C307 in the presence of KI; complete ref 2. This material is available free of charge via the Internet at http://pubs.acs.org.

AUTHOR INFORMATION

Corresponding Author
*E-mail: selvaraj24@hotmail.com.

ACKNOWLEDGMENT

We thank Prof. P. Natarajan for his constant encouragement and for many informative discussions during the course of this work. This work was supported by University Grants Commission, Government of India by the grant no.:31-138/2005(SR) to C.S. P.R. thanks Department of Science and Technology, Government of India for the financial support under IRHPA programme.

REFERENCES

(1) Long, F. H.; Lu, H.; Shi, X.; Eisenthal, K. B. *Chem. Phys. Lett.* **1991**, *185*, 47–52.
(2) Garrett, B. C.; et al. *Chem. Rev.* **2005**, *105*, 355–389.
(3) Braun, C. L.; Scott, T. W. *J. Phys. Chem.* **1987**, *91*, 4436–4438.
(4) Sagar, D. M.; Bain, C. D.; Verlet, J. R. R. *J. Am. Chem. Soc.* **2010**, *132*, 6917–6919.
(5) Wang, W.; Zafiriou, O. C.; Chan, I.; Zepp, R. G.; Blough, N. V. *Environ. Sci. Technol.* **2007**, *41*, 1601–1607.
(6) Fleming, G.; Martin, J.; Breton, J. *Nature* **1988**, *333*, 190–192.
(7) Fox, M. A. *Photochem. Photobiol.* **1990**, *52*, 617–627.
(8) Selvaraju, C.; Ramamurthy, P. *Chem.—Eur. J.* **2004**, *10*, 2253–2262.
(9) Fragneto, G.; Rheinstadter, M. *C. R. Phys.* **2007**, *8*, 865–883.
(10) Ehrler, O. T.; Neumark, D. M. *Acc. Chem. Res.* **2009**, *42*, 769–777.
(11) Gangotri, P.; Gangotri, K. M. *Int. J. Energy Res.* **2010**, *34*, 1155–1163.
(12) Gauduel, Y.; Berrod, S.; Migus, A.; Yamada, N.; Antonetti, A. *Biochemistry* **1988**, *27*, 2509–2518.
(13) Kalyanasundaram, K. *Photochemistry in Microheterogeneous System*; Academic Press: Orlando, FL, 1987.
(14) Fendler, J. H. *Membrane Mimetic Chemistry*; Wiley-Interscience: New York, 1982.

(15) Stam, J. V.; Imans, F.; Viaene, L.; De Schryver, F. C.; Evans, C. H. *J. Phys. Chem. B* **1999**, *103*, 5160–5166.
(16) Bagchi, B. *Chem. Rev.* **2005**, *105*, 3197–3219.
(17) Bhattacharyya, K. *Acc. Chem. Res.* **2003**, *36*, 95–101.
(18) Bhattacharyya, K. *Chem. Commun.* **2008**, 2848–2857.
(19) Datta, A.; Pal, S. K.; Mandal, D.; Bhattacharyya, K. *J. Phys. Chem. B* **1998**, *102*, 6114–6117.
(20) Balasubramanian, S.; Bagchi, B. *J. Phys. Chem. B* **2001**, *105*, 12529–12533.
(21) Sen, P.; Roy, D.; Mondal, S. K.; Sahu, K.; Ghosh, S.; Bhattacharyya, K. *J. Phys. Chem. A* **2005**, *109*, 9716–9722.
(22) Burai, T. N.; Datta, A. *J. Phys. Chem. B* **2009**, *113*, 15901–15906.
(23) Modig, K.; Liepinsh, E.; Otting, G.; Halle, B. *J. Am. Chem. Soc.* **2004**, *126*, 102–114.
(24) Marchi, M.; Sterpone, F.; Ceccarelli, M. *J. Am. Chem. Soc.* **2002**, *124*, 6787–6791.
(25) Murarka, R. K.; Head-Gordon, T. *J. Phys. Chem. B* **2008**, *112*, 179–186.
(26) Lang, M. J.; Jordanides, X. J.; Song, X.; Fleming, G. R. *J. Chem. Phys.* **1999**, *110*, 5884–5893.
(27) Furse, K. E.; Corcelli, S. A. *J. Chem. Theory Comput.* **2009**, *5*, 1959–1967.
(28) Nilsson, L.; Halle, B. *Proc. Natl. Acad. Sci. U.S.A* **2005**, *102*, 13867–13872.
(29) Maroncelli, M. *J. Mol. Liq.* **1993**, *57*, 1–37.
(30) Pal, S. K.; Peon, J.; Bagchi, B.; Zewail, A. H. *J. Phys. Chem. B* **2002**, *106*, 12376–12395.
(31) Jiminez, R.; Fleming, G. R.; Kumar, P. V.; Maroncelli, M. *Nature* **1994**, *369*, 471–473.
(32) Nandi, N.; Bagchi, B. *J. Phys. Chem. B* **1997**, *101*, 10954–10961.
(33) Nandi, N.; Bhattacharyya, K.; Bagchi, B. *Chem. Rev.* **2000**, *100*, 2013–2045.
(34) Zhao, L.; Pal, S. K.; Xia, T.; Zewail, A. H. *Angew. Chem., Int. Ed.* **2004**, *43*, 60–63.
(35) Pal, S. K.; Zewail, A. H. *Chem. Rev.* **2004**, *104*, 2099–2123.
(36) Peon, J.; Pal, S. K.; Zewail, A. H. *Proc. Natl. Acad. Sci. U.S.A.* **2002**, *99*, 10964–10969.
(37) Bhattacharyya, S. M; Wang, Z.-G.; Zewail, A. H. *J. Phys. Chem. B* **2003**, *107*, 13218–13228.
(38) Tavernier, H. L.; Laine, F.; Fayer, M. D. *J. Phys. Chem. A* **2001**, *105*, 8944–8957.
(39) Kumbhakar, M.; Nath, S.; Mukherjee, T.; Pal, H. *J. Chem. Phys.* **2004**, *120*, 2824–2834.
(40) Maroncelli, M.; Fleming, G. R. *J. Chem. Phys.* **1987**, *86*, 6221–6240.
(41) Fee, R. S.; Maroncelli, M. *Chem. Phys.* **1994**, *183*, 235–247.
(42) Nad, S.; Kumbhakar, M.; Pal, H. *J. Phys. Chem. A* **2003**, *107*, 4808–4816.
(43) Arbeloa, T. L.; Arbeloa, F. L.; Tapia, M. J.; Arbeloa, I. L. *J. Phys. Chem.* **1993**, *97*, 4704–4707.
(44) Chen, L.; Wood, P. D.; Mnyusiwalla, A.; Marlinga, J.; Johnston, L. J. *J. Phys. Chem. B* **2001**, *105*, 10927–10935.
(45) Wood, P. D.; Johnston, L. J. *J. Phys. Chem. A* **1998**, *102*, 5585–5591.
(46) Priyadarsini, K. I.; Mittal, J. P.; Naik, D. B.; Moorthy, P. N. *J. Chem. Soc., Faraday Trans.* **1991**, *87*, 269–272.
(47) Jones, G., II; Griffin, S. F.; Choi, C.; Bergmark, W. R. *J. Org. Chem.* **1984**, *49*, 2705–2708.
(48) Dempster, D. N.; Morrow, T.; Quinn, M. F. *J. Photochem.* **1973**, *2*, 329–341.
(49) Arce, R.; Garcia, C.; Oyola, R.; Pinero, L.; Nieves, I.; Cruz, N. *J. Photochem. Photobiol., A* **2003**, *154*, 245–257.
(50) Kumbhakar, M.; Goel, T.; Nath, S.; Mukherjee, T.; Pal, H. *J. Phys. Chem. B* **2006**, *110*, 25646–25655.
(51) Chakrabarty, D.; Hazra, P.; Sarkar, N. *J. Phys. Chem. A* **2003**, *107*, 5887–5893.
(52) Quitevis, E. L.; Marcus, A. H.; Fayer, M. D. *J. Phys. Chem.* **1993**, *97*, 5762–5769.
(53) Maiti, N. C.; Krishna, M. M. G.; Britto, P. J.; Periasamy, N. *J. Phys. Chem. B* **1997**, *101*, 11051–11060.
(54) Dutt, G. B. *J. Phys. Chem. B* **2002**, *106*, 7398–7404.
(55) Chakrabarty, D.; Chakraborty, A.; Seth, D.; Hazra, P.; Sarkar, N. *J. Chem. Phys.* **2005**, *122*, 184516–1.
(56) Kumbhakar, M.; Nath, S.; Pal, H.; Sapre, A. V.; Mukherjee, T. *J. Chem. Phys.* **2003**, *119*, 388–399.
(57) Migus, A.; Gauduel, Y.; Martin, J. L.; Antonetti, A. *Phys. Rev. Lett.* **1987**, *58*, 1559–1562.
(58) Cassol, R.; Ge, M.-T.; Ferrarini, A.; Freed, J. H. *J. Phys. Chem. B* **1997**, *101*, 8782–8789.
(59) Sarkar, N.; Datta, A.; Das, S.; Bhattacharyya, K. *J. Phys. Chem.* **1996**, *100*, 15483–15486.
(60) Kumbhakar, M.; Goel, T.; Mukherjee, T.; Pal, H. *J. Phys. Chem. B* **2004**, *108*, 19246–19254.
(61) Janata, E.; Schuler, R. H. *J. Phys. Chem.* **1982**, *86*, 2078–2084.
(62) Ghosh, H. N. *J. Phys. Chem. B* **1999**, *103*, 10382–10387.
(63) Senthilkumar, S.; Nath, S.; Pal, H. *Photochem. Photobiol.* **2004**, *80*, 104–111.
(64) Satpati, A. K.; Kumbhakar, M.; Nath, S.; Pal, H. *Photochem. Photobiol.* **2009**, *85*, 119–129.
(65) Ramakrishna, G.; Ghosh, H. N. *J. Phys. Chem. A* **2002**, *106*, 2545–2553.
(66) Pal, S.; Balasubramanian, S.; Bagchi, B. *J. Phys. Chem. B* **2003**, *107*, 5194–5202.
(67) Sen, P.; Mukherjee, S.; Halder, A.; Bhattacharyya, K. *Chem. Phys. Lett.* **2004**, *385*, 357–361.
(68) Streletzky, K.; Phillies, G. D. J. *Langmuir* **1995**, *11*, 42–47.
(69) Datta, A.; Mandal, D.; Pal, S. K.; Das, S.; Bhattacharyya, K. *J. Mol. Liq.* **1998**, *77*, 121–129.
(70) Pal, S. K.; Sukul, D.; Mandal, D.; Sen, S.; Bhattacharyya, K. *Chem. Phys. Lett.* **2000**, *327*, 91–96.
(71) Vajda, S.; Jimenez, R.; Rosenthal, S. J.; Fidler, V.; Fleming, G. R.; Castner, E. W., Jr. *J. Chem. Soc., Faraday Trans* **1995**, *91*, 867–873.
(72) Jesenska, A.; Sykora, J.; Olzynska, A.; Brezovsky, J.; Zdrahal, Z.; Damborsky, J.; Hof, M. *J. Am. Chem. Soc.* **2009**, *131*, 494–501.
(73) Mandal, U.; Adhikari, A.; Dey, S.; Ghosh, S.; Mondal, S. K.; Bhattacharyya, K. *J. Phys. Chem. B* **2007**, *111*, 5896–5902.